IOP Publishing Journal of Physics A: Mathematical and Theoretical
J. Phys. A: Math. Theor. **57** (2024) 325303 (17pp) https://doi.org/10.1088/1751-8121/ad65a2

Helicity of magnetic fields associated with non-relativistic electron vortex beams

N Alsaawi[1,2,*], V E Lembessis[2], A Lyras[2], M Babiker[3] and J Yuan[3]

[1] Department of Physics, College of Science, Qassim University, PO Box 6644, Buraidah 51452, Saudi Arabia
[2] Department of Physics and Astronomy, College of Science, King Saud University, PO Box 2455, Riyadh 11451, Saudi Arabia
[3] School of Physics, Engineering and Technology, University of York, YO10 5DD, Heslington, United Kingdom

E-mail: no.alsaawi@qu.edu.sa

Received 31 January 2024; revised 8 July 2024
Accepted for publication 19 July 2024
Published 29 July 2024

Abstract

The helicities of the magnetic fields associated with non-relativistic electron vortex beams are considered for radially extended Bessel modes. Investigating the helicity density of this system lies in realizing the unique electric and magnetic properties of electron vortex beams that influence their interactions with matter. We have evaluated the vector potential components needed for the derivation of the magnetic helicity density and found that this has a non-zero distribution. This is attributed entirely to the cylindrically symmetric density flux of the electron beam, which scales with the winding number ℓ. It is also related to the magnetic moments of the electron oriented along the z-direction, giving rise to the z-component of the magnetic field. We obtain different helicity distributions for different signs of winding number $\pm\ell$, which confirms the chiral character of the magnetic fields associated with the electron vortex beam. The physical consequences of taking the spin current density into consideration are also examined. This allows a comparison to be made between the evaluated total current helicities, one with and one without including the spin-polarization.

Keywords: vortex beams, electrons, helicity, chirality, current density

* Author to whom any correspondence should be addressed.

1. Introduction

Recent years have witnessed the experimental realization of electron vortex modes as twisted electron beams [1–3]. These are beams of freely propagating electrons endowed with a well-defined orbital angular momentum (OAM) about their propagation axis [4, 5]. Such beams, like their optical counterparts [6], are hollow and could carry a large amount of quantized angular momentum in the direction of their propagation. Each vortex beam is characterized by a wavefront with a quantized topological structure arising from a singularity in phase taking the form $e^{i\ell\phi}$, with ϕ being the azimuthal angle about the beam axis and ℓ an integer quantum number known as the winding number that determines the OAM of the vortex which is given by $\ell\hbar$ per electron. Like optical vortex beams, electron vortex beams are accompanied also by electromagnetic fields [7]. This is because electrons possess a half-integer spin, an electric charge and an associated magnetic moment. Also, electron vortex beams can probe much smaller structures than is possible with the optical vortex beams due to their very small de Broglie wavelengths. Until recently, the spin degrees of freedom of electron vortex beams have not been investigated in detail and there has been a lack of experimental techniques to study them. However, this may well be about to change because of the development in highly-spin-polarized electron sources [8, 9].

Electron vortices have applications in various areas, including quantum information, nuclear physics and nanoscience. For example, chiral matter responds differently to the application of electron vortex beams of different handedness $+\ell$ or $-\ell$, i.e. interaction processes are sensitive to the relative handedness of the electron vortex beam. As a result, they provide useful new information not only about chiral crystals [10], but also about the magnetic properties of matter [2, 11–19].

In addition to their electrical currents, the spin-polarized electron beams with or without vortex properties can also give rise to spin currents which are of great interest in spintronics. Also the recent detection of orbital Hall effects [20–22] confirms the importance of OAM in condensed matter and the possible emergence of the area of 'Orbitronics' [23]. Further studies of the magnetic fields associated with the spin and OAM of electron vortex beams also have implications for future developments in condensed matter physics.

One way to understand the properties of the electron vortex beams is to consider the fields associated with such beams, as these fields often mediate the interaction between the electron vortex beams and the surrounding matter. Here we focus on the magnetic helicity and the current helicity associated with electron vortex beams. Helicity measures the linkage or twisting of the field lines [24, 25], and provides a mathematical tool for interpreting the handedness of magnetic fields. It is widely applied to different topics such as gravitational waves [26], magnetohydrodynamics, magnetic reconnection, astronomy studies (e.g. active galactic regions, and planetary magnetospheres), and coronal mass ejections, as reviewed by Brown *et al* [27] and Buechner & Pevtsov [28]. It has also featured prominently in the characterization of the topological properties of magnetic materials [29]. The magnetic helicity and the electromagnetic helicity are distinct but they are related constituent parts of the total helicity of a system comprising both electromagnetic fields and matter [30]. Recently some authors have sought to explore and clarify the helicity and the chirality of the electromagnetic field associated with the optical vortex beams [31, 32]. These properties play crucial roles in understanding the interaction of chiral light with matter. For example, the chirality of light has the ability to detect and separate molecules of opposite chirality [33], and to increase the capacity and selectivity which improve the optical information storage and transfer [34]. However, the helicities of the magnetic fields associated with the non-relativistic electron vortex beam have not been studied before. Our goal in this paper is to report our investigations leading to results in this context.

The structure of the paper is as follows. In section 2 we consider the system of the electron vortex beams and define the magnetic and current helicities associated with its magnetic field. In section 3, we consider the current helicity and the magnetic helicity of the vortex beam in the non-relativistic regime with the electron vortex represented as a Bessel mode. In subsection 3.3 we include the spin current density as a component of the non-relativistic electron vortex current density and evaluate the helicities associated with the magnetic field in that case. Finally, section 4 contains our conclusions and further comments.

2. Background

2.1. Non-relativistic electron vortex beams

Freely propagating electron vortices that exhibit the required quantized angular momentum have been described by the Schrodinger equation [5] for low and medium electron energy beams and by Dirac equations at relativistic energies. In this paper, we restrict ourselves to the non-relativistic regime in which most experiments have been carried out. The simplest electron vortex beam solution of the Schrodinger equation is the Bessel mode. An electron Bessel beam of energy $\mathcal{E}$ propagating in the z-direction has a wavefunction given in cylindrical coordinates $\mathbf{r} = (\rho, \phi, z)$ by [7, 35]:

$$\psi(\mathbf{r}, t) = N_\ell J_\ell(k_\perp \rho)\, \mathrm{e}^{\mathrm{i}k_z z} \mathrm{e}^{\mathrm{i}\ell\phi} \mathrm{e}^{-\mathrm{i}\mathcal{E}t/\hbar}, \tag{1}$$

where ℓ is the winding number, $k_\perp$ and k_z are the transverse and longitudinal components of the electron wave-vector $\mathbf{k}$ such that $\mathcal{E} = \hbar^2 k^2/2m_e$, where m_e is the electron mass, while N_ℓ is a normalization constant. The Bessel beam has the distinct features of z-independence in the transverse beam structure, apart from a kinetic phase factor $\mathrm{e}^{\mathrm{i}k_z z}$. This 'non-diffracting' feature of Bessel beams has been experimentally demonstrated [36]. Our evaluation will accordingly be based on experimentally relevant parameters.

The transverse (i.e. in-plane) structure of an ideal Bessel beam has an infinite set of concentric rings, hence it is not square integrable. This presents a numerical difficulty of finding out the appropriate expression for the normalization constant (N_ℓ). For that, one needs to go for either truncated Bessel beams [37] or solutions of the paraxial approximate version of the Schrödinger equation, such as a Laguerre–Gaussian solution having a Gaussian envelope [5]. However, these solutions necessarily contain diffraction effects, so would add further complications on taking into account of the z-dependence without shedding additional light on the physics being investigated here. In our work we focus on Bessel beams where we can disregard their propagation along the z-axis. As we see, the normalization issue can be circumvented by looking at the beam intensity of the Bessel rings which is indeed square integrable and in fact has a constant value [38].

2.2. Current and magnetic helicities

The helicity density of the field lines is a measure of the degree of twisting or coiling of the field lines in a given region of space. It has its origin in fluid dynamics where the field line is described by its velocity field $\mathbf{v}$ and the helicity density is defined as a dot product of the velocity field and the vorticity of the velocity vector ($\nabla \times \mathbf{v}$). For solenoidal fields, the space integral of the helicity density is a measure of the average topological linkage of the vorticity vector field lines [25]. This important topological property applies to both the vector potential

A and the magnetic field **B** and gives rise to the definitions of the following related helicity densities [39, 40]: The Magnetic helicity density η is defined as

$$\eta = \mathbf{A} \cdot \nabla \times \mathbf{A} = \mathbf{A} \cdot \mathbf{B} \tag{2}$$

and the Current helicity density χ is

$$\chi = \mathbf{B} \cdot (\nabla \times \mathbf{B}) = \mu_0 \mathbf{B} \cdot \mathbf{J} \tag{3}$$

where **J** is the electric current density. The last step follows from the Ampere's circuital law with μ_0 the vacuum permeability. These two helicity densities describe the topological features of the magnetic field and current density flow, respectively.

As the vector field **A** is gauge-dependent, this means that the magnetic helicity density is also gauge-dependent. Thus the interpretation of the magnetic helicity needs careful consideration of the gauge used [41]. Here we fix the gauge as $\nabla \cdot \mathbf{A} = 0$. The current helicity density and its space integral are manifestly gauge invariant, and we can evaluate the total current helicity per unit length which is an integral of the current helicity density over the transverse plane.

3. Evaluations of the helicities

The evaluations of the current helicity and the magnetic helicity require as input the magnetic field and the vector potential of the Bessel mode. Fortunately, the magnetic field has already been derived by Lloyd *et al* [7] and we leave the derivation of the corresponding vector potential to section 3.2. We now evaluate the current density of a single unpolarized electron vortex beam. The equivalent current density due to spin-polarized electron vortex is considered next, in section 3.3.

Using the Bessel mode wavefunction given in equation (1), we can easily deduce the beam current density as follows [7]:

$$\tilde{\mathbf{J}}_\ell(\mathbf{r}) = -\frac{e|N_\ell|^2\hbar}{m_e} J_\ell^2(k_\perp \rho)\left(\frac{\ell}{\rho}\hat{\boldsymbol{\phi}} + k_z \hat{\mathbf{z}}\right). \tag{4}$$

In the following numerical evaluation, we take for the longitudinal momentum the value $k_z = 2.3 \times 10^{12}\mathrm{m}^{-1}$, corresponding to 300 keV accelerating voltage, which is typical for the electron microscopes used in electron vortex beam experiments [2]. The transverse wave vector component $k_\perp$ is taken to be two orders of magnitude smaller than this, i.e. $2.3 \times 10^{10}\mathrm{m}^{-1}$. Lloyd *et al* [7] used the current density in equation (4) to arrive at the following expressions for the magnetic field components:

$$B_\phi(\rho) = \frac{e\mu_0\hbar k_z|N_\ell|^2}{m_e\rho}\int_0^\rho J_\ell^2(k_\perp\rho')\,\rho'\mathrm{d}\rho', \tag{5}$$

$$B_z(\rho) = \frac{e\mu_0\hbar|N_\ell|^2\ell}{m_e}\int_\rho^\infty \frac{J_\ell^2(k_\perp\rho')\,\mathrm{d}\rho'}{\rho'}. \tag{6}$$

It has been shown that the B_ϕ component exhibits an oscillatory form which decreases at larger radial distances and its magnitude decreases as the winding number increases. Its expression contains the Bessel function of the first kind squared, therefore it does not depend on the sign of the winding number. This is to be expected as it is due to the longitudinal motion of the electron vortex beams (i.e. the second term inside the bracket in equation (4)). The oscillatory feature is due to the set of rings in the Bessel beam, with increasing radius. In contrast, B_z depends explicitly on ℓ, therefore a reversal of the sign of the winding number inverts its sign. This is

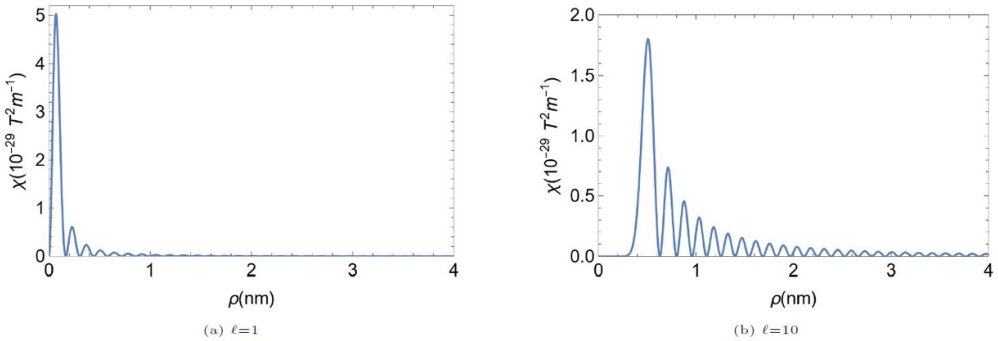

Figure 1. The current helicity density of an infinite radial extent Bessel beam corresponding to 300 keV accelerating voltage and current 1 nA with (a) $\ell = 1$, and (b) $\ell = 10$. The radial oscillatory behavior dominates at larger radial distances for a higher winding number associated with a lower helicity density value. Because of the proportionality of χ to ℓ, the current helicity plots for the negative winding number will be inverted with respect to the horizontal axis.

related to the azimuthal components of the current density shown in equation (4). The circular motion of the electron in each ring of the Bessel mode is equivalent to a current loop and this gives rise to a magnetic moment pointing along the beam axis. These magnetic moments are responsible for the z-component of the magnetic field whose size depends on the angular momentum of the circulating electronic flux.

3.1. Current helicity

Inserting the magnetic field expressions equations (5) and (6) into equation (3) leads to the following expression for the current helicity density

$$\chi = \frac{e^2\mu_0^2\hbar^2 k_z |N_\ell|^4 \ell}{m_e^2 \rho}\left[\int_\rho^\infty \frac{J_\ell^2(k_\perp \rho')\,\mathrm{d}\rho'}{\rho'}\frac{\partial}{\partial\rho}\left(\int_0^\rho J_\ell^2(k_\perp\rho')\,\rho'\mathrm{d}\rho'\right) - \int_0^\rho J_\ell^2(k_\perp\rho')\,\rho'\mathrm{d}\rho'\frac{\partial}{\partial\rho}\left(\int_\rho^\infty \frac{J_\ell^2(k_\perp\rho')}{\rho'}\mathrm{d}\rho'\right)\right], \tag{7}$$

where the first term is the axial helicity density which arises due to the coupling of z-component of the current density to the longitudinal magnetic field component and the second term due to the azimuthal helicity density which arises from the coupling of the azimuthal current density component to the azimuthal magnetic field component.

Figure 1 displays the radial distribution of the current helicity density for Bessel beams with $\ell = 1$, and 10. It is seen that the current helicity density exhibits an oscillatory form similar to the one exhibited by the magnetic field components. Thus on increasing the winding number we have a reduced first peak and decreasing oscillations at larger radial distances ρ. In view of the magnetic field expressions and the Bessel function property $J_{-\ell}(x) = (-1)^\ell J_\ell(x)$ which holds for integer ℓ [42], this indicates that $J_\ell = J_{-\ell}$ for even ℓ, and for odd ℓ, we have $J_\ell = -J_{-\ell}$. We conclude that the current helicity density and, subsequently, the total current helicity for negative winding numbers both become negative.

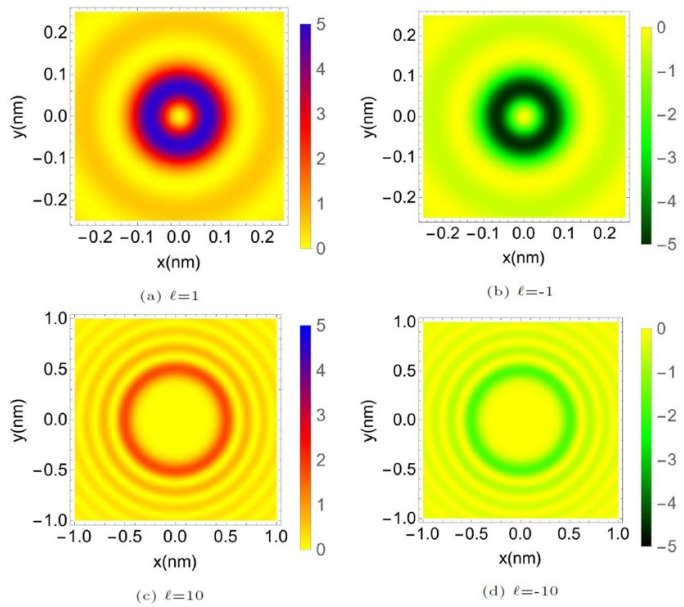

Figure 2. The in-plane current helicity density distributions for Bessel beams with (a) $\ell = 1$, (b) $\ell = -1$, (c) $\ell = 10$, and (d) $\ell = -10$. See the text for the other parameters used to evaluate these figures.

The two-dimensional current helicity density distribution are further displayed in figure 2 to reveal the azimuthal dependence. Figure 2(a) displays the current helicity of the Bessel beam with winding number $\ell = 1$ and figure 2(b) with negative winding number $\ell = -1$. The cases $\ell = \pm 10$ are also shown in figures 2(c) and (d). It is clear from equation (3) that the current helicity density depends on the sign of ℓ and thus the regions where the current helicity density is high (in blue) in figure 2(a) are replaced by regions of low helicity density (in black) in figure 2(b) and vice versa. These findings suggest that we have different distributions for left and right handed helicity density, as expected since the axial component of the magnetic field is proportional to ℓ.

The total current helicity per unit length is found by an integration over the entire transverse plane as

$$\mathcal{H}_C = \int_S \mathbf{B} \cdot (\nabla \times \mathbf{B})\, \rho \mathrm{d}\rho \mathrm{d}\phi, \tag{8}$$

where the integration over ϕ gives 2π. The total current helicity for each ℓ value was calculated for the range from zero up to $\ell = 10$, with the aid of the numerical integration method of Double Exponential Oscillatory in Mathematica. The results are shown in figure 3. We see an almost linear dependence of the total current helicity on the winding number ℓ. This shows that the double integral in equation (7), when integrated over the transverse plane, has a very weak ℓ-dependence. This is consistent with our expectation that the winding properties of the current density vector field shown in equation (4) is dependent on the winding number of the Bessel beam, i.e. its azimuthal component.

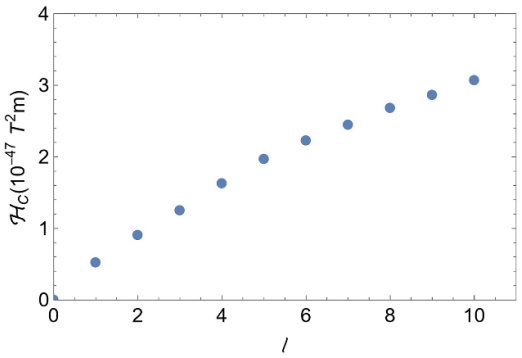

Figure 3. The variations of the total current helicity of an infinite radial extent Bessel beams with the winding number ℓ, plotted here for values from $\ell = 0$ to $\ell = 10$.

3.2. Magnetic helicity density

A direct evaluation of the vector potential of the electron vortex beam makes use of the magnetic field expressions already evaluated. In cylindrical coordinates these magnetic field components are related to the vector potential components as follows

$$\mathbf{B} = -\frac{\mathrm{d}A_z}{\mathrm{d}\rho}\hat{\boldsymbol{\phi}} + \frac{1}{\rho}\frac{\mathrm{d}\left(\rho A_\phi\right)}{\mathrm{d}\rho}\hat{\mathbf{z}}. \tag{9}$$

The vector potential depends only on ρ and has a radial component equal to zero. Inserting the magnetic field expression equations (5) and (6), we obtain two separate equations in the form

$$\frac{\mathrm{d}A_z}{\mathrm{d}\rho} = -\frac{e\mu_0\hbar k_z|N_\ell|^2}{m_e\rho}\int_0^\rho J_\ell^2\left(k_\perp\rho'\right)\rho'\mathrm{d}\rho', \tag{10}$$

$$\frac{1}{\rho}\frac{\mathrm{d}\left(\rho A_\phi\right)}{\mathrm{d}\rho} = \frac{e\mu_0\hbar|N_\ell|^2\ell}{m_e}\int_\rho^\infty \frac{J_\ell^2\left(k_\perp\rho'\right)\mathrm{d}\rho'}{\rho'}. \tag{11}$$

Solving these using Mathematica's built-in function DSolve for the solution of the first order differential equations, we have:

$$A_\phi(\rho) = \frac{e\mu_0\hbar|N_\ell|^2\rho}{4m_e}\left(1 - \frac{1}{\ell^2\Gamma^2(\ell)}\left(4^{1-\ell}\left(\rho k_\perp\right)^{2\ell}\Gamma^2(\ell+1)\Gamma(2\ell+1)\,{}_2\tilde{F}_3\left[\left\{\ell, \frac{1}{2}+\ell\right\};\right.\right.\right.$$
$$\left.\left.\left.\{1+\ell, 1+2\ell, 2+\ell\}; -\rho^2k_\perp^2\right]\right)\right), \tag{12}$$

$$A_z(\rho) = \frac{e\mu_0\hbar|N_\ell|^2k_z\rho^2}{4m_e}\left(J_{\ell-1}\left(k_\perp\rho\right)J_{\ell+1}\left(k_\perp\rho\right) - J_{\ell+1}^2\left(k_\perp\rho\right) - J_\ell^2\left(k_\perp\rho\right)\right.$$
$$+ J_\ell\left(k_\perp\rho\right)J_{\ell+2}\left(k_\perp\rho\right) + 4^{-\ell}\left(\rho k_\perp\right)^{2\ell}\Gamma(2+2\ell)\,{}_2\tilde{F}_3\left[\left\{1+\ell, \frac{3}{2}+\ell\right\};\right.$$
$$\left.\left.\times\ \{2+\ell, 2+\ell, 2+2\ell\}; -\rho^2k_\perp^2\right]\right), \tag{13}$$

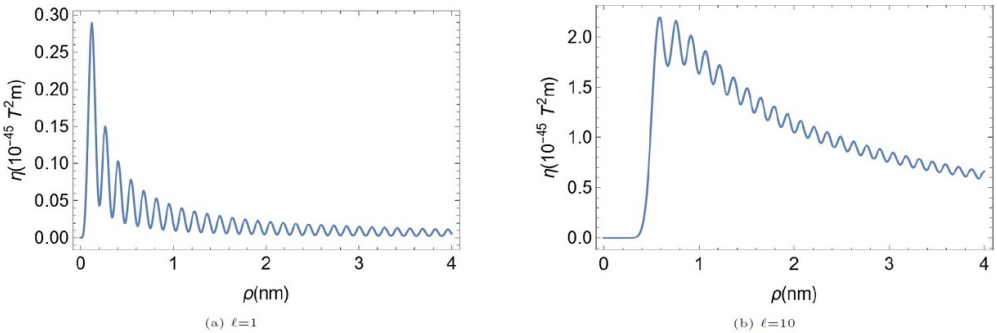

Figure 4. The magnetic helicity density of an infinite radial extent Bessel beams with (a) $\ell = 1$, and (b) $\ell = 10$. The first peak has the highest value in the case of $\ell = 10$ and each peak represents a ring in the following distribution plots. The magnetic helicity plots for the negative winding number will be inverted with respect to the horizontal axis.

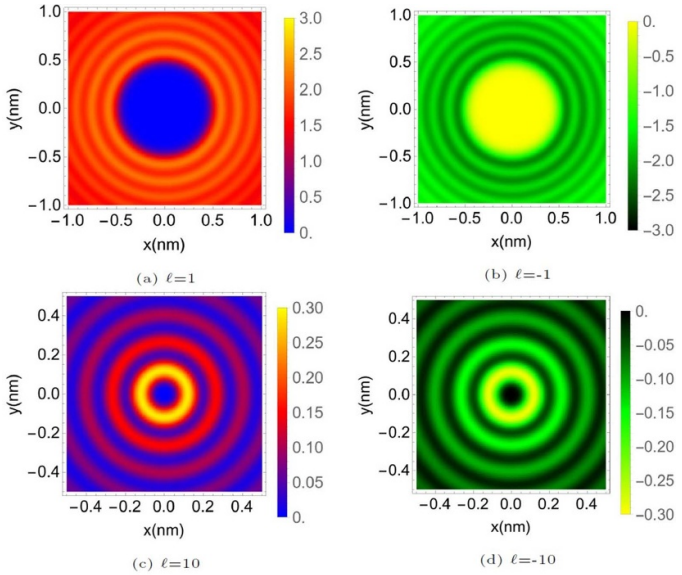

Figure 5. The in-plane magnetic helicity density distribution for Bessel beams with (a) $\ell = 1$, (b) $\ell = -1$, (c) $\ell = 10$, and (d) $\ell = -10$.

where ${}_p\tilde{F}_q[a_1 \ldots a_p; b_1 \ldots b_q; z]$ is the regularized hypergeometric function. We have verified that the Coulomb gauge condition $\nabla \cdot \mathbf{A} = 0$ is fulfilled by this choice of vector potential components. By taking the curl of the vector potential in cylindrical coordinates, we can confirm that they reproduce the correct magnetic field components.

Using the above expressions, equations (12) and (13), in equation (2), we obtain the magnetic helicity density plots shown in figures 4 and 5. It is seen that these resemble those of the current helicity shown in figures 1 and 2, in that they have a 'damped' oscillatory form. The 'damping' is faster for small values of ℓ, while there is a region of nearly constant intensity in the vicinity of the center with an increasing value of ℓ.

Also, it is important to note from the figures that a chirality behavior is exhibited here. By comparing figure 5(a) with 5(b) one can see that the regions of high magnetic helicity density are replaced by regions of low magnetic helicity density, and vice versa for all Bessel beams with the same absolute winding number but with the opposite sign.

Finally, both helicities, current and magnetic, are zero in the case of a zero winding number, but for larger ℓ values, there are significant differences between the two as the current helicity becomes zero at specific ρ values.

3.3. Spin current contribution

We now turn to consider the contributions of the spin of the electron to the helicities of a non-relativistic electron vortex beam. The current density $\mathbf{J}_s$ associated with a spin-polarized beam mode is defined as follows [43, 44]

$$\tilde{\mathbf{J}}_s = \nabla \times \left(\Psi^\dagger \mathbf{m} \Psi\right), \tag{14}$$

where

$$\mathbf{m} = -\frac{g_e \mu_B \mathbf{s}}{\hbar}, \tag{15}$$

in which $\mu_B = \frac{e\hbar}{2m_e}$ stands for the Bohr magneton, g_e is a dimensionless constant (called the g-factor) which is approximately equal to -2 in the case of the electron, and $\mathbf{s} = \frac{\hbar}{2}\boldsymbol{\sigma}$ is the spin angular momentum of the electron. Here Ψ represents the electron vortex beam wave function given in equation (1) multiplied by either of the eigenspinors of the spin operator s_z defined as

$$\chi_+ = \begin{pmatrix} 1 \\ 0 \end{pmatrix}, \qquad \chi_- = \begin{pmatrix} 0 \\ 1 \end{pmatrix}. \tag{16}$$

Equation (14) can then be written as

$$\tilde{\mathbf{J}}_s = \frac{e\hbar}{2m_e} \nabla \times \left(\psi_\ell^* \chi_\pm^\dagger \sigma_z \psi_\ell \chi_\pm\right), \tag{17}$$

where σ_z is the third Pauli matrix

$$\sigma_z = \begin{pmatrix} 1 & 0 \\ 0 & -1 \end{pmatrix}. \tag{18}$$

On performing the matrix multiplication on the right hand side of equation (17), we obtain the contribution of the electron spin to the current density

$$\tilde{\mathbf{J}}_{s=\pm\frac{1}{2}} = \mp \frac{e\hbar |N_\ell|^2}{2m_e} \frac{\partial}{\partial \rho} \left(J_\ell^2 (k_\perp \rho)\right) \hat{\boldsymbol{\phi}}. \tag{19}$$

The total current density, including the spin contribution is then given by

$$\tilde{\mathbf{J}}_{\ell, s=\pm\frac{1}{2}} = \tilde{\mathbf{J}}_\ell + \tilde{\mathbf{J}}_s. \tag{20}$$

Substituting from equation (4), we obtain

$$\tilde{\mathbf{J}}_{\ell, s=\pm\frac{1}{2}} = -\frac{e|N_\ell|^2 \hbar}{m_e} \left\{ \left[\frac{\ell J_\ell^2 (k_\perp \rho)}{\rho} \pm \frac{1}{2} \frac{\partial}{\partial \rho} \left(J_\ell^2 (k_\perp \rho)\right) \right] \hat{\boldsymbol{\phi}} + J_\ell^2 (k_\perp \rho) k_z \hat{\mathbf{z}} \right\}. \tag{21}$$

The spin current density is seen to have only an azimuthal component which contributes a term additional to the original current density equation (4) to generate the total azimuthal current density. The axial component of the current density is unaffected, so that this leads only to a

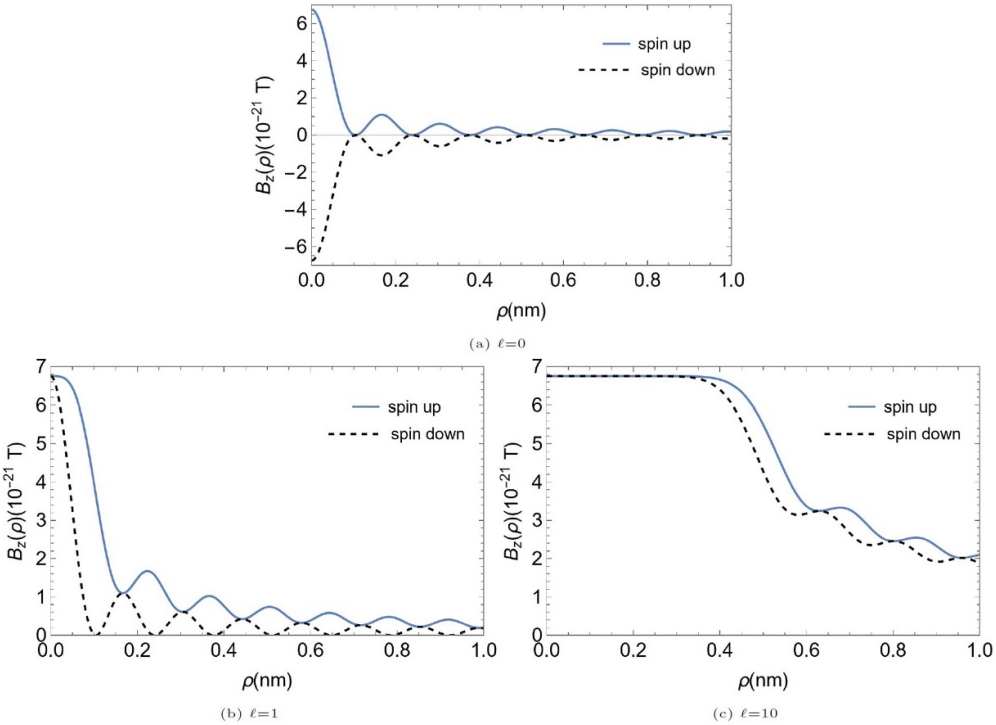

Figure 6. The axial magnetic field of an infinite Bessel beams with (a) $\ell = 0$, (b) $\ell = 1$, and (c) $\ell = 10$ respectively, taking the spin current into consideration . The field plots are oscillatory, drop off to zero faster for smaller value of the winding number. Note that we have an axial magnetic field component for $\ell = 0$ when we take the spin current contribution into account.

modification of the ϕ component of the current density equation (4). Since the current density is proportional to the curl of the magnetic field by appeal to equation (3) we find that the azimuthal component of the magnetic field remains unchanged, while the axial component is modified as follows

$$B_{z,s=\pm\frac{1}{2}}(\rho) = \frac{e\mu_0\hbar|N_\ell|^2}{2m_e}\left[1 \pm J_\ell^2(k_\perp\rho) - \frac{{}_2F_3\left[\{\ell,\ell+\frac{1}{2}\};\{\ell+1,\ell+1,2\ell+1\};-\rho^2k_\perp^2\right]4^{-\ell}}{(\rho k_\perp)^{-2\ell}\,\ell^2\Gamma^2(\ell)}\right]. \tag{22}$$

Figure 6 displays the radial variations of the axial component of the magnetic field as given by equation (22) for non-relativistic infinite Bessel beams with $\ell = 0, 1$ and 10. These plots clearly show that we now have different field amplitudes for the two spin states at the vortex core and the difference between the two plots decreases with increasing ℓ. We see that $(B_z)_{s=\frac{-1}{2}}$ takes lower values than $(B_z)_{s=\frac{1}{2}}$, and this is very obvious for $\ell = 0$ as the OAM contribution to B_z is zero. From equation (19), one can see that the peak current density contributions to the magnetic field come from the highest gradient of the electron beam density of the spin-polarized Bessel mode and the zeros of the spin current density and hence B_z correspond to the peaks in the electron beam density. By comparison, the current density due to the OAM of the vortex beams is proportional to the electron density of the beam (equation (4)), so the spin- and

orbital-angular-momentum-derived B_z distributions are peaked at different radiii, even though both show the ripple structures due to the contribution of individual rings in the Bessel beam. This is why the ripple structures of the B_z distribution shown in figures 6(b) and (c) for the oppositely spin-polarized vortex beams with $\ell = 1, 10$, respectively, are out of phase. Another difference for the spin-derived and OAM-derived B_z as shown in equation (22) is their different behaviours at the vortex core. As shown in figure 6(c), the contribution to B_z at the vortex core only comes from the vortex structure, hence is the same for oppositely spin-polarized beams.

We can now substitute the magnetic field expressions equations (5) and (22) in equation (3) in order to determine the effects of including the spin current on the current helicity density. The results for vortex beams for which $\ell = 0, \pm 1$, and ± 10 are displayed in figure 7. The significant point here is the non-vanishing χ for the case of $\ell = 0$ as a result of taking the spin current into account. While for $\ell = 0$ the plots for the two different values of s appear as mirror images with respect to the horizontal axis. The plots for $\ell > 0$ have markedly different features. If we consider the plots (b) (spin up) and (d) (spin down) we see that they look symmetric with respect to the z-axis corresponding to values $3/2$ and $-3/2$ for the sum $(\ell + s)$. Similarly for the other two plots, (c) and (e) corresponding to values $21/2$ and $-21/2$. The derived structures do not have spherical symmetry but cylindrical symmetry. So the total angular momentum j is probably irrelevant. What may be relevant is the j_z eigenvalue directed along the z-axis. The different positions of the peaks in the ripple structure of oppositely spin-polarized vortex beams of the same topological charge ℓ can be traced back to the difference in the respective spin-derived and OAM-derived contribution to the current helicity density for the spin-polarized Bessel vortex beam, in a similar way as we have found for the corresponding B_z distribution we have just discussed.

On the other hand, the total current helicity results for spin-polarized Bessel vortex beams show a simpler dependence on the winding number ℓ as shown in figure 8. For both spin states, the total current helicity increased as a result of increasing the winding number and took on a larger value in the spin up state. It is interesting to see that, in contrast to the case shown in figure 3, for $\ell = 0$ the total helicity is not zero because of the spin contribution. The result is not entirely surprising as the charge and current distribution which are responsible for the generation of all the physical effects in this work have a cylindrical symmetry, so what really matters here is neither the total angular momentum J nor the OAM ℓ but the J_z eigenvalue along the z-axis. Of course, the dependence is not exact because spin-derived current density and the OAM-derived current density do not scale in exactly the same way as s and ℓ, so the difference between total current helicities of the two oppositely spin-polarized Bessel vortex beams varies slightly as a function of the winding number ℓ. Having seen how the inclusion of the spin current leads to a modified magnetic field, we now consider the corresponding vector potential which, too, includes the effects of the spin current. This is needed in order to explore the corresponding magnetic helicity density. Once again, an analysis based on equation (9) reveals that the azimuthal component of the vector potential now becomes:

$$A_{\phi,s=\pm\frac{1}{2}}(\rho) = \frac{e\mu_0\hbar|N_\ell|^2\rho}{4m_e}\left[1 - \frac{{}_2\tilde{F}_3\left[\left\{\ell, \frac{1}{2}+\ell\right\};\{1+\ell, 1+2\ell, 2+\ell\};-\rho^2k_\perp^2\right]}{4^{-1+\ell}(\rho k_\perp)^{-2\ell}\ell^2\Gamma^2(\ell)\Gamma^{-2}(\ell+1)\Gamma^{-1}(2\ell+1)}\right.$$
$$\left. \pm \left(J_\ell^2(k_\perp\rho) - J_{\ell-1}(k_\perp\rho)J_{\ell+1}(k_\perp\rho)\right)\right], \tag{23}$$

while the axial vector potential component is not affected. Substituting the vector potential components equations (12) and (23) in the magnetic helicity density equation (2), we obtain as results the plots exhibited in figure 9. These show the magnetic helicity densities for the

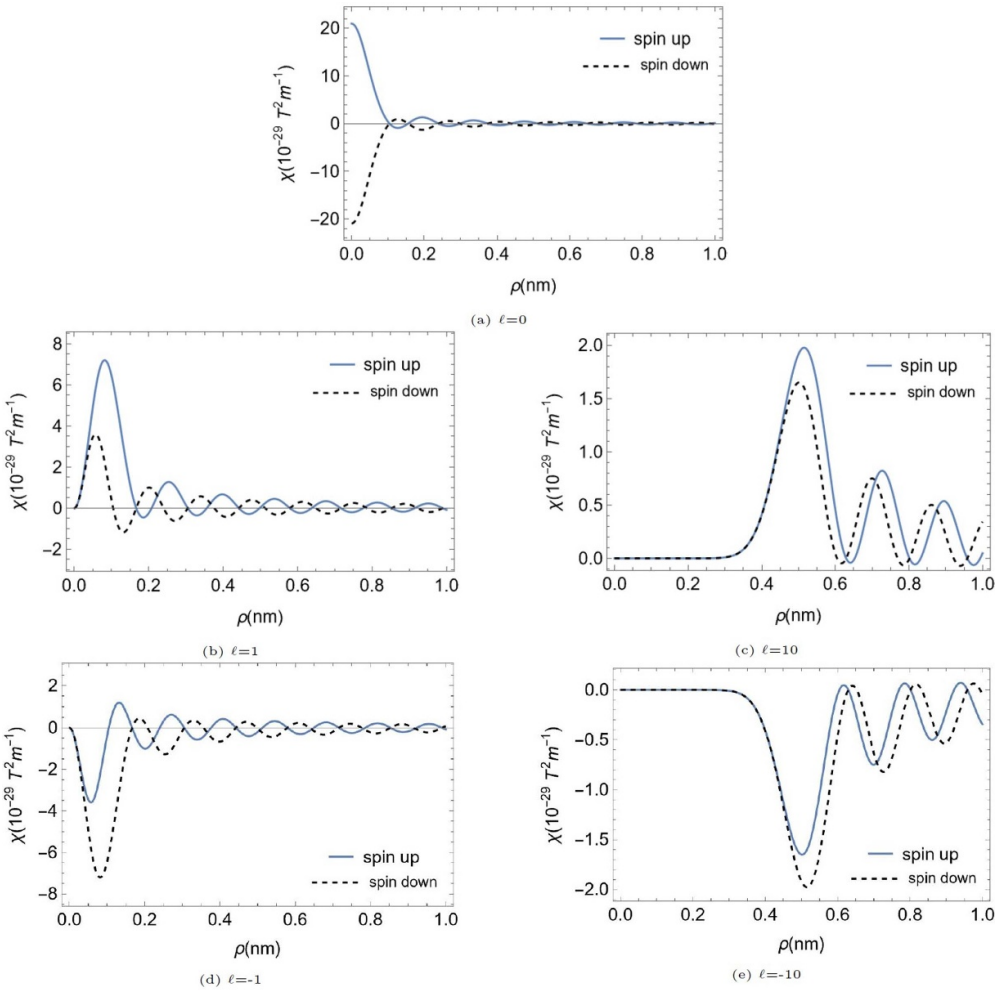

Figure 7. The current helicity density of an infinite non-relativistic electron Bessel beam with (a) $\ell = 0$, (b) $\ell = 1$, (c) $\ell = 10$, (d) $\ell = -1$, and (e) $\ell = -10$, respectively, taking the spin current into consideration. The most important of these is how the difference between the current helicity density reduced for larger values of ℓ and the minima at the centre of the beam becomes wider. We include the current helicity plots for beams with a negative winding number here since they are not exactly the opposite of their positive counterpart; for example, χ for $\ell = 1, s = +1/2$ reflected with respect to the horizontal axis to χ for $s = -1/2$ in the case of $\ell = -1$. This is also true in the case of magnetic helicity density.

winding numbers $\ell = 0, \pm 1$ and ± 10. These agree qualitatively with the current helicity density results in the previous subsection on the following aspects: First, both of them have an oscillatory form. Second, in the case of a zero winding number, the spin-up magnetic helicity is the opposite of the spin-down magnetic helicity. Third, the magnitude of the magnetic helicity for the spin-down Bessel vortex beam is always less than that for the spin-up Bessel vortex beam of the same OAM, and their difference decreases for higher values of ℓ. Finally,

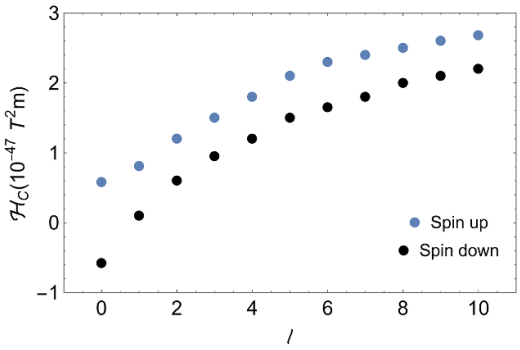

Figure 8. The variations with the winding number ℓ of the total current helicity of infinite spin polarized Bessel beams for winding numbers ranging between $\ell = 0$ and $\ell = 10$.

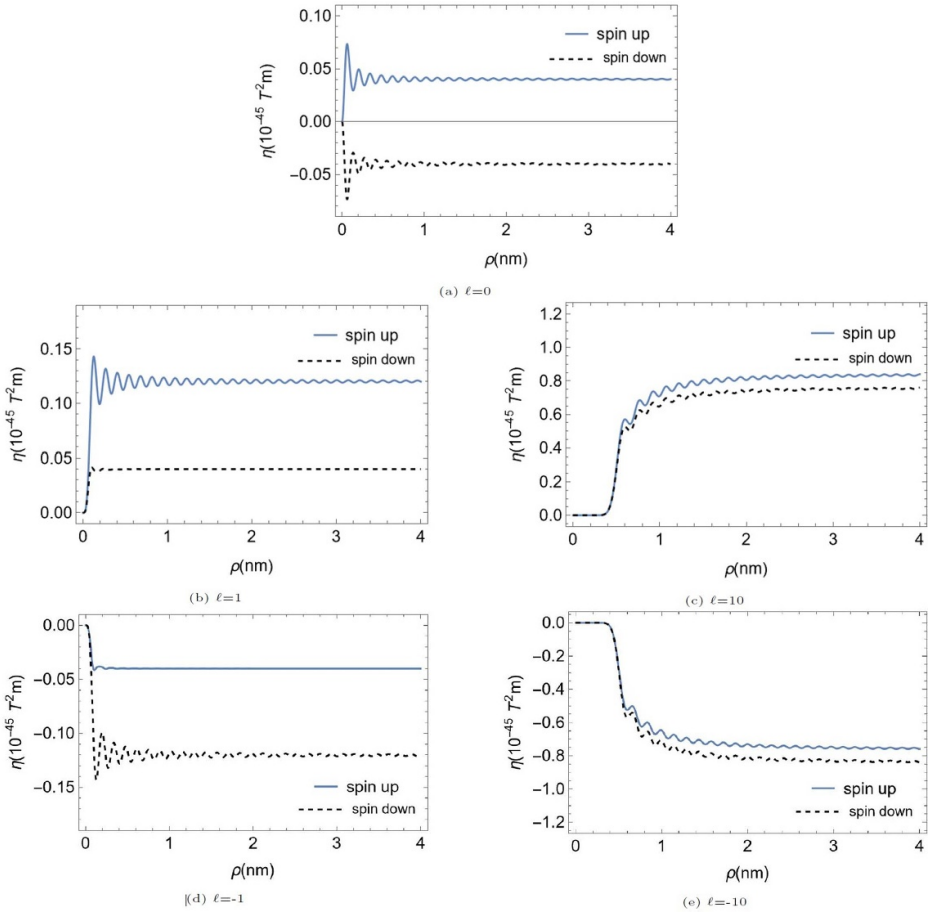

Figure 9. The radial variations of the magnetic helicity density of an infinite non-relativistic electron Bessel beam taking the spin current into consideration (a) $\ell = 0$, (b) $\ell = 1$, (c) $\ell = 10$, (d) $\ell = -1$, and (e) $\ell = -10$, respectively. Here the solid and dashed lines are used to identify the spin orientation. The main message is the reversing behaviour of the solid and dashed lines in figure (b) and (d) which is due to the relative orientation of the spin with respect to that of the OAM.

increasing the winding number causes an increase in the magnetic helicity density and, hence, the total magnetic helicity.

4. Conclusions

In conclusion, we have used the knowledge of the electric current and associated magnetic field of electron vortex beams to evaluate for the first time, to the best of our knowledge, the magnetic and current helicities associated with a non-relativistic electron Bessel vortex beam. The current helicity density was explored for different winding numbers and noted the increase in its value and a shift of the first peak position towards larger radial distances as the winding number increases. We have, also, derived analytical expressions for the vector potential components and we used them to study the magnetic helicity density and its dependence on the winding number of the electron vortex beam.

We have also shown that when the two spin states of the electron are taken into consideration, something that is not usually done in non-relativistic treatments, we obtain different helicity densities associated with the non-relativistic electron vortex beam. This is clearly shown in the corresponding plots in the case of electron Bessel vortex modes. The reason for this difference lies in the fact that the spin polarized beams are characterized by a non-vanishing spin current density, which is not present when the spin degrees of freedom are not taken into account. The inclusion of spin brings in a new term in the expression of the axial magnetic field component; by contrast, the azimuthal magnetic field component is the same for both spin states. As shown in the corresponding plots, when we take into account the spin the system shows a genuine chirality in the sense that when we consider simultaneously $\ell \to -\ell$ and $\sigma \to -\sigma$ the helicities are different. Our work has also shown that when the winding number increases the magnetic fields associated with electron vortex beams having different spin states converge to common values. This is an indication that as the OAM increases its contribution to the current density dominates over the one originating from spin. As a result, the helicities for different spin values will converge as ℓ gets larger.

We have also explored the total current helicity and emphasized that it increases with ℓ, whether one takes the electrons spin into account or not. The effect of spin is about the same magnitude as that from a unit of OAM. We have treated the spin-derived current density and the OAM-derived current density to be additive. This may still be approximately appropriate for 300 keV electron beams studied here, but a proper consideration of the effect of spin-polarization will wait for a relativistic theory of electron vortex beams, a subject of further research.

We have shown that the fields associated with non-relativistic electron vortex beams exhibit chirality by comparing the distribution plots for the positive and negative orders of the same winding number. The chiral nature of the electron vortex enables the detection and analysis of chiral materials, thereby providing information about their spatial arrangement, structural properties, and potential biological or chemical activities.

An important parameter in spatially resolved analysis using vortex electron beam is the achievable resolution. As it is well known that the eigenstates of electron vortex beams generally have dimensions which scale with OAM, still atomic scale resolutions have been demonstrated experimentally in such an optimised situation [45]. However, in this paper we have evaluated the helicity of the electromagnetic fields associated with the electron vortex beam, so their overall size is certainly larger than the overall size of the beam. For the realistic parameters we have used, we have shown that the extent of the field is still in the nanometre scale. Furthermore, the resolution that can be achieved is not always a function of the overall size

of the beam, but could be determined by the sharpest feature in the structured illumination, if deconvolution processing can be applied. In that regard, it is worth to note that vortex beams can generate focal features whose dimensions can approach or supersede those of a non-structured Gaussian beam [37, 46].

As to the evaluated helicity of the beam, this is related to the steady state electric and magnetic fields associated with the electron vortex beam, and, as such, it is different from that arising from the time-dependent electric and magnetic fields associated with electron magnetic circular dichroism in inelastic electron energy loss spectroscopy. The helicity of the beam may be more relevant to the process of elastic scattering of chiral materials by vortex beams and the polarisation of any chiral electromagnetic objects, which is a subject that requires further investigations.

Finally, chirality could be used to encode and process quantum information, which could lead to advancements in quantum computing and communications. Further exploration and experimental investigations are needed to fully understand and utilize the potential of these chiral properties.

Data availability statement

No new data were created or analysed in this study.

ORCID iDs

N Alsaawi https://orcid.org/0000-0001-6515-7912
V E Lembessis https://orcid.org/0000-0002-2000-7782
M Babiker https://orcid.org/0000-0003-0659-5247
J Yuan https://orcid.org/0000-0002-6240-7151

References

[1] Uchida M and Tonomura A 2010 Generation of electron beams carrying orbital angular momentum *Nature* **464** 737–9
[2] Verbeeck J, Tian H and Schattschneider P 2010 Production and application of electron vortex beams *Nature* **467** 301–4
[3] McMorran B, Agrawal A, Anderson I, Herzing A, Lezec H, McClelland J and Unguris J 2011 Electron vortex beams with high quanta of orbital angular momentum *Science* **331** 192–5
[4] Lloyd S, Babiker M, Thirunavukkarasu G and Yuan J 2017 Electron vortices: Beams with orbital angular momentum *Rev. Mod. Phys.* **89** 035004
[5] Bliokh K Y *et al* 2017 Theory and applications of free-electron vortex states *Phys. Rep.* **690** 1–70
[6] Allen L, Beijersbergen M, Spreeuw R and Woerdman J 1992 Orbital angular momentum of light and the transformation of laguerre-gaussian laser modes *Phys. Rev.* A **45** 8185–9
[7] Lloyd S, Babiker M, Yuan J and Kerr-Edwards C 2012 Electromagnetic vortex fields, spin and spin-orbit interactions in electron vortices *Phys. Rev. Lett.* **109** 254801
[8] Kuwahara M, Takeda Y, Saitoh K, Ujihara T, Asano H, Nakanishi T and Tanaka N 2011 Development of spin-polarized transmission electron microscope *J. Phys.: Conf. Ser.* 298 012016
[9] Pan D and Xu H 2023 Polarizing free electrons in optical near fields *Phys. Rev. Lett.* **130** 186901
[10] Juchtmans R, Béché A, Abakumov A, Batuk M and Verbeeck J 2015 Using electron vortex beams to determine chirality of crystals in transmission electron microscopy *Phys. Rev.* B **91** 094112
[11] Idrobo J and Pennycook S 2011 Vortex beams for atomic resolution dichroism *J. Electron Microsc.* **60** 295–300
[12] Lloyd S, Babiker M and Yuan J 2012 Quantized orbital angular momentum transfer and magnetic dichroism in the interaction of electron vortices with matter *Phys. Rev. Lett.* **108** 074802

[13] Schattschneider P, Schaffer B, Ennen I and Verbeeck J 2012 Mapping spin-polarized transitions with atomic resolution *Phys. Rev.* B **85** 134422
[14] Asenjo-Garcia A and García de Abajo F J 2014 Dichroism in the interaction between vortex electron beams, plasmons and molecules *Phys. Rev. Lett.* **113** 066102
[15] Harvey T, Pierce J, Chess J and McMorran B 2015 Demonstration of electron helical dichroism as a local probe of chirality (https://doi.org/10.48550/arXiv.1507.01810)
[16] Gallatin G and McMorran B 2012 Propagation of vortex electron wave functions in a magnetic field *Phys. Rev.* A **86** 012701
[17] Bliokh K, Schattschneider P, Verbeeck J and Nori F 2012 Electron vortex beams in a magnetic field: a new twist on landau levels and aharonov-bohm states *Phys. Rev.* X **2** 041011
[18] Greenshields C, Stamps R and Franke-Arnold S 2012 Vacuum faraday effect for electrons *New J. Phys.* **14** 103040
[19] Babiker M, Yuan J and Lembessis V E 2015 Electron vortex beams subject to static magnetic fields *Phys. Rev.* A **91** 013806
[20] Sala G, Wang H, Legrand W and Gambardella P 2023 Orbital hanle magnetoresistance in a 3 d transition metal *Phys. Rev. Lett.* **131** 156703
[21] Lyalin I, Alikhah S, Berritta M, Oppeneer P and Kawakami R 2023 Magneto-optical detection of the orbital hall effect in chromium *Phys. Rev. Lett.* **131** 156702
[22] Choi Y-G, Jo D, Ko K-H, Go D, Kim K-H, Park H G, Kim C, Min B-C, Choi G-M and Lee H-W 2023 Observation of the orbital hall effect in a light metal ti *Nature* **619** 52-56
[23] Bernevig B, Hughes T and Zhang S 2005 Orbitronics: The intrinsic orbital current in p -doped silicon *Phys. Rev. Lett.* **95** 066601
[24] Moreau J 1961 Constantes d'un îlot tourbillonnaire en fluide parfait barotrope *C. R. Hebd. Seances Acad. Sci.* **252** 2810–2
[25] Moffatt H K 1969 The degree of knottedness of tangled vortex lines *J. Fluid Mech.* **35** 117–29
[26] Bini D, Mashhoon B and Obukhov Y N 2022 Gravitomagnetic helicity *Phys. Rev.* D **105** 064028
[27] Brown M, Canfield R, Field G, Kulsrud R, Pevtsov A, Rosner R and Seehafer N 1999 Magnetic helicity in space and laboratory plasmas: editorial summary *Geophys. Monograph-American Geophys. Union* **111** 301–4
[28] Büchner J and Pevtsov A 2003 Magnetic helicity *Adv. Space Res.* **32** 1817 (available at: https://hdl.handle.net/11858/00-001M-0000-0014-EE71-0)
[29] Nagaosa N and Tokura Y 2013 Topological properties and dynamics of magnetic skyrmions *Nat. Nanotechnol.* **8** 899–911
[30] Fernandez-Corbaton I 2021 Total helicity of electromagnetic fields and matter *Phys. Rev.* B **103** 54406
[31] Koksal K, Babiker M, Lembessis V E and Yuan J 2021 Chirality and helicity of linearly-polarised laguerre-gaussian beams of small beam waists *Opt. Commun.* **490** 126907
[32] Forbes K and Andrews D 2018 Optical orbital angular momentum: twisted light and chirality *Opt. Lett.* **43** 435–8
[33] Zhao Y, Saleh A, Van De Haar M, Baum B, Briggs J, Lay A, Reyes-Becerra O and Dionne J 2017 Nanoscopic control and quantification of enantioselective optical forces *Nat. Nanotechnol.* **12** 1055–9
[34] Le Feber B, Rotenberg N and Kuipers L 2015 Nanophotonic control of circular dipole emission *Nat. Commun.* **6** 6695
[35] Schattschneider P and Verbeeck J 2011 Theory of free electron vortices *Ultramicroscopy* **111** 1461–8
[36] Grillo V, Karimi E, Gazzadi G C, Frabboni S, Dennis M R and Boyd R W 2014 Generation of nondiffracting electron bessel beams *Phys. Rev.* X **4** 011013
[37] Thirunavukkarasu G, Mousley M, Babiker M and Yuan J 2017 Normal modes and mode transformation of pure electron vortex beams *Phil. Trans. R. Soc.* A **375** 20150438
[38] Durnin J 1987 Exact solutions for nondiffracting beams i the scalar theory *J. Opt. Soc. Am.* A **4** 651
[39] Subramanian K and Brandenburg A 2006 Magnetic helicity density and its flux in weakly inhomogeneous turbulence *Astrophys. J.* **648** 71
[40] Berger M and Field G 1984 The topological properties of magnetic helicity *J. Fluid Mech.* **147** 133–48
[41] Prior C and Yeates A R 2014 On the helicity of open magnetic fields *Astrophys. J.* **787** 100
[42] Potter M C 1978 *Mathematical Methods in the Physical Sciences* (Prentice-Hall)

[43] Landau L, Lifshitz E, Sykes J, Bell J and Rose M 1958 Quantum mechanics, non-relativistic theory of course of theoretical physics *Phys. Today* **3** 11
[44] Mita K 2000 Virtual probability current associated with the spin *Am. J. Phys.* **68** 259–64
[45] Béché A, Juchtmans R and Verbeeck J 2017 Efficient creation of electron vortex beams for high resolution stem imaging *Ultramicroscopy* **178** 12–19
[46] Huo P, Yu R, Liu M, Zhang H, Lu Y and Xu T 2024 Tailoring electron vortex beams with customizable intensity patterns by electron diffraction holography *Opto-Electron. Adv.* **7** 230184–1